

# Reconstruction of Accelerating Nonlinear $f(T)$ Gravity Models via Hybrid Scale Factor: Cosmological Dynamics and Bayesian Evidence

Suraj Kumar Behera \*

Department of Mathematics, School of Advanced Sciences, VIT-AP University,  
Beside AP Secretariat, Amaravati, 522241, Andhra Pradesh, India.

Pratik P. Ray †

Department of Mathematics, School of Advanced Sciences, VIT-AP University,  
Beside AP Secretariat, Amaravati, 522241, Andhra Pradesh, India and  
Pacif Institute of Cosmology and Selfology (PICS), Sagara, Sambalpur 768224, Odisha, India.

## Abstract

This study offers a comprehensive reconstruction of  $f(T)$  gravity model with three distinct nonlinear as well as novel forms employing a hybrid scale factor to depict the expansion history of the universe starting from early decelerated epoch to late-time accelerated evolution. Model parameters are rigorously constrained using the Monte Carlo Markov Chain (MCMC) analysis with the help of Bayesian statistics and incorporating late-time observations from BAO and Patheon+SH0ES. The investigation of dynamical parameters such as the equation of state parameter and cosmological parameters indicates alignment with an accelerated expansion phase in both the present and late time epochs. Validation is conducted by assessing the energy conditions, verifying the feasibility of the model forms with particular emphasis on the violation of the strong energy condition that indicates dark energy dominance in modified gravity scenarios. This investigation has been instrumental in determining models that remain consistent with cosmological observations and theoretical requirements. The reconstructed forms of the model effectively mimic  $\Lambda$ CDM at late times, providing significant insights into possible extensions of general relativity and bolstering  $f(T)$  gravity theory as a robust explanation for cosmic acceleration.

PACS numbers:

**Keywords:**  $f(T)$  Gravity; Hybrid scale factor; Monte Carlo Markov Chain; EoS Parameter; Energy Conditions

## I. INTRODUCTION

The observation of accelerated cosmic expansion signifies a landmark development in modern cosmology, fundamentally reshaping our comprehension of large-scale structure and energy composition of the universe. Type Ia Supernovae were the initial to observe this phenomenon [1, 2], and precise measurements of the Cosmic Microwave Background (CMB) [3, 4] and Baryon Acoustic Oscillations (BAO) [5, 6] verified it later. A more comprehensive inquiry into the primary causes of the accelerated expansion has been stimulated by accumulating the observational evidence, which has demonstrated it as an accepted feature of our universe [7]. This unexplained phenomena has been ascribed to an enigmatic component that is dark energy (DE), which constitutes a substantial amount of the overall energy budget of the universe [8]. In the beginning, a cosmological constant  $\Lambda$  is put forward as the most fundamental type of DE in the standard cosmological model,  $\Lambda$ CDM model, which is used as the framework [9–11]. Despite its achievements with the large-scale structure of the universe [12],  $\Lambda$ CDM has theoretical problems. These include the coincidence problem, which arises question that the near-equality of matter and DE densities in the current epoch [13], and the cosmological constant problem, in which quantum field theory predicts a vacuum energy that is substantially greater than what is observed [14].

Because of these constraints, a number of modified theories of gravity have been introduced to explain the acceleration phenomena of the universe without relying on a cosmological constant [15, 16]. Teleparallel gravity is one of the more appealing types of modified theories. Instead of implementing the traditional spacetime metric  $g_{\mu\nu}$  to convey gravitational effects, this gravity uses a tetrad field  $e_1^\mu$ . Torsion, which is generated by the tetrads, is enough to represent the gravity. This approach led to the establishment of  $f(T)$  gravity, where torsion takes the place of curvature to produce a flat spacetime framework. and the Teleparallel equivalent of general relativity (TEGR) [17–19].  $f(T)$  gravity has a major advantage, which is its second-order field equations rather than the fourth-order in  $f(R)$ . Without using DE, this theory has been excellent at describing late-time cosmic acceleration, thereby making it an excellent contender to tackle unanswered questions in cosmology. Tamanini and Boehmer [20] examined the

\*Electronic address: [skbehera.researches@gmail.com](mailto:skbehera.researches@gmail.com)

†Electronic address: [pratik.chika9876@gmail.com](mailto:pratik.chika9876@gmail.com); [pratik.ray@vitap.ac.in](mailto:pratik.ray@vitap.ac.in)

dynamics of  $f(T)$  gravity models, paying special attention to their cosmological implications and stability. The literature [21] discusses an interacting cosmic fluid with  $f(T)$  gravity that is characterized by a generalized Chaplygin gas with viscosity. In their study of different aspects of  $f(T)$  gravity, Dent et al. [22] explored how minor deviations from general relativity might show up in cosmological measurements. In the case of a charged black hole,  $f(T)$  gravity provides an analytical solution [23]. Geng et al. [24] analyzed the stability of cosmological models while focusing on the dynamics of  $f(T)$  gravity in the presence of a perfect fluid. Also, some other investigations in the framework of  $f(T)$  gravity are large-scale structure [25], accelerated expansion [26], finite time singularity [27, 28].

The cosmic transition from early deceleration to present accelerated expansion has been investigated with a hybrid scale factor, which combines exponential and power-law behaviours to model a smooth evolution of the universe. Mishra and Tripathy[29] developed an anisotropic dark energy model within Bianchi type V spacetime, employing a hybrid scale factor to characterize the cosmic transition from early deceleration to late-time acceleration. An anisotropic dark energy model in Bianchi type V spacetime with two non-interacting fluids-cosmic strings and dark energy is developed using a hybrid scale factor in the Ref.[30]. Misra, Ray and Pacif[31] examined anisotropic dark energy cosmological models within Bianchi type V spacetime by considering three general forms of the scale factor, including a hybrid one. Mishra et al.[32] examined Bianchi type V anisotropic cosmologies inside the extended  $f(R, T)$  gravity framework. Narawade, Koussour, and Mishra[?] explored an anisotropic cosmological model in the framework of  $f(Q, T)$  gravity, employing a hybrid scale factor with model parameters constrained by Hubble, BAO, and Pantheon datasets.

In this study, we investigate the dynamics and behaviour of three well-motivated non-linear forms of  $f(T)$  such as  $f(T) = T - \frac{a}{(-T/6)^n} + b(\frac{-T}{6})^m$ ,  $f(T) = T - aT_0[(1 + \frac{T^2}{T_0^2})^{-n} - 1]$ , and  $f(T) = T + aT_0 \frac{(T^2/T_0^2)^n}{1+(T^2/T_0^2)^n}$  considering the hybrid scale factor with constraints on its parameters through the Monte Carlo Markov Chain (MCMC) approach using Bayesian statistics. The evolutionary behavior is verified with the equation of state parameter, and also, the energy conditions are examined. This paper follows a format like: in Sec.II, the field equations of  $f(T)$  are formulated, and also, the dynamical parameters and the equation of state (EoS) parameter ( $\omega$ ) are derived. Sec.III discusses the hybrid scale factor and the Hubble model derived from it. Model parameters are constrained by fitting with observational datasets through the MCMC algorithm in sec.IV. The dynamics of the newly reconstructed  $f(T)$  models are investigated in sec.V by plotting dynamical parameters. The energy conditions of the models are examined in sec.VI. Finally, in the sec.VII, the conclusions of this study have been discussed, followed by the future scope of research.

## II. MATHEMATICAL FRAMEWORK FOR FIELD EQUATIONS

In the Teleparallel formulation of gravity, by employing the tetrads as the fundamental dynamical variables, instead of the metric tensor, General Relativity (GR) can be reconstructed in an equivalent way [33]. At each point in spacetime, the tetrad field creates a basis  $e_\mu(x)$ , where  $\mu$  varies from 0 to 3, representing four linearly independent vectors. It will be feasible to expand each tetrad vector  $e_\mu$  in the coordinate basis to get the tetrad components  $e_\mu^a$ . Hence, the orthogonality relation between the tetrads and the spacetime metric is expressed as

$$g_{\mu\nu} = \eta_{ab} e_\mu^a e_\nu^b \quad (1)$$

where  $g_{\mu\nu}$  is the metric tensor and  $\eta_{ab} = \text{diag}(1, -1, -1, -1)$  represents the Minkowski metric. The inverse relation takes the form

$$E_a^\mu e_\mu^b = \delta_a^b \quad (2)$$

and the tetrad is  $e = \det[e_\mu^a] = \sqrt{-g}$ .

The Wittenböck connection [34] is defined as  $\Gamma^\sigma_{\mu\nu} \equiv E_a^\sigma \partial_\mu e_\nu^a$  which leads to a non-vanishing torsion tensor

$$T^\sigma_{\mu\nu} \equiv \Gamma^\sigma_{\nu\mu} - \Gamma^\sigma_{\mu\nu} = E_a^\sigma \partial_\mu e_\nu^a - E_a^\sigma \partial_\nu e_\mu^a \quad (3)$$

This allows us to achieve the contorsion tensor as

$$K^{\mu\nu}_\sigma = \frac{1}{2}(T_\sigma^{\mu\nu} + T^{\nu\mu}_\sigma - T^{\mu\nu}_\sigma) \quad (4)$$

The torsion scalar is then determined to be

$$T \equiv S_\sigma^{\mu\nu} T_{\mu\nu}^\sigma \quad (5)$$

where the superpotential tensor is defined as

$$S_\sigma^{\mu\nu} = \frac{1}{2} [K^{\mu\nu}{}_\sigma + \delta_\sigma^\mu T^{\alpha\nu}{}_\alpha - \delta_\sigma^\nu T^{\alpha\mu}{}_\alpha] \quad (6)$$

This ensures that the GR and TEGR actions will produce identical field equations.

In the framework of TEGR, the gravitational Lagrangian depends linearly on the torsion scalar  $T$ . This is generalized by the  $f(T)$  gravity framework, which substitutes  $T + f(T)$  for  $T$ . The formula for the action [35] is defined by

$$A = \frac{1}{16\pi G} \int d^4x e [T + f(T) + \mathcal{L}_m] \quad (7)$$

Here,  $G$  is the gravitational constant and  $\mathcal{L}_m$  is the total matter Lagrangian density. We use natural units throughout this study by setting  $8\pi G = \kappa^2 = c = 1$ .

Taking the variation of the action (7) with regard to the tetrad fields leads to the corresponding formula of modified field equations, mentioned as,

$$e^{-1} \partial_\mu (e E_a^\rho S_\rho^{\mu\nu}) [1 + f_T] + E_a^\rho S_\rho^{\mu\nu} \partial_\mu (T) f_{TT} + \frac{1}{4} E_a^\nu T - E_a^\sigma T_{\mu\sigma}^\rho S_\rho^{\nu\mu} [1 + f_T] + \frac{1}{4} E_a^\nu f(T) = 4\pi G E_a^\rho \mathcal{T}_\rho^\nu, \quad (8)$$

where,  $f_T$  and  $f_{TT}$  are first and second derivatives of  $f(T)$  with respect to  $T$  respectively. Also,  $\mathcal{T}_\rho^\nu$  indicates the total matter energy-momentum tensor of perfect fluid in the context.

We consider a spatially flat Friedman-Lemaître-Robertson-Walker (FLRW) universe for cosmological applications, which is expressed by the line elements

$$ds^2 = dt^2 - a^2(t)(dx^2 + dy^2 + dz^2) \quad (9)$$

Here,  $a(t)$  is the scale factor. Moreover, we choose the diagonal tetrad  $(1, a(t), a(t), a(t))$ , and substituting into the field equations' formula (8), the Friedman equations modified for  $f(T)$  gravity are obtained as

$$3H^2 = 8\pi G(\rho_m + \rho_r) - \frac{f(T)}{2} + T f_T \quad (10)$$

$$\dot{H} = -\frac{4\pi G(\rho_m + \rho_r + p_m + p_r)}{1 + f_T + 2T f_{TT}} \quad (11)$$

Here onward from this field equations we use  $f = f(T)$ ,  $f_T$  and  $f_{TT}$  are first and second derivatives of  $f(T)$  with respect to  $T$  and  $H \equiv \frac{\dot{a}}{a}$ .  $\rho_m$  and  $\rho_r$  represent the energy densities of matter and radiation, respectively, while  $p_m$  and  $p_r$  denote the corresponding pressures. In this context of  $f(T)$  gravity, the effective DE density and pressure are given by

$$\rho_{de} \equiv \frac{1}{16\pi G} [-f + 2T f_T] \quad (12)$$

$$p_{de} \equiv -\frac{1}{16\pi G} \left[ \frac{-f + T f_T - 2T^2 f_{TT}}{1 + f_T + 2T f_{TT}} \right] \quad (13)$$

where we use the relation  $T = -6H^2$ . The effective EoS parameter for the DE sector is thus expressed as

$$\omega_{de} = -1 + \frac{(f_T + 2T f_{TT})(-f + T + 2T f_T)}{(1 + f_T + 2T f_{TT})(-f + 2T f_T)} \quad (14)$$

A time-dependent EoS parameter is crucial for investigating the accelerated expansion of the universe because it provides a more flexible parametrization with regard to the redshift. To make this analysis simpler, we use a hybrid scale factor in the section that follows.

### III. PARAMETRIZATION OF THE HYBRID SCALE FACTOR

Some observations of the present universe indicate that the power-law expansion and the de-sitter solution emerge as appropriate choices for the scale factor. Both the power-law and exponential forms of the scale factor exhibit a constant deceleration parameter. In this study, we examine a certain scale factor, namely the hybrid scale factor [29] that inherently results in a constant deceleration parameter at late times. The expression for the hybrid scale factor can be presented as

$$a(t) = e^{\lambda t} t^\beta \quad (15)$$

where  $\lambda$  and  $\beta$  are positive constants. This form blends two different evolutionary behaviors: a power-law expansion with  $t^\beta$  and exponential expansion with  $e^{\lambda t}$ . Early cosmic dynamics are dominated by the power-law term, whereas later eras are dominated by the exponential term. The hybrid scale factor eventually evolves to a stage in which the exponential component governs the dynamics, precisely simulating the accelerated expansion of the universe.

Additionally, this formulation elegantly connects multiple cosmological phases: the standard exponential (de-sitter) expansion is recovered for  $\beta = 0$  and the model reduces to a pure power-law expansion for  $\lambda = 0$ . Thus, the hybrid scale factor delivers a cohesive explanation of the evolution of the universe by providing a natural mechanism to describe a cosmic shift from an early decelerated phase to a late-time accelerated period. The Hubble parameter derived from this model is given by

$$H(z) = \lambda + \frac{\lambda}{W\left(\frac{\lambda(\frac{1}{z+1})^{1/\beta}}{\beta}\right)} \quad (16)$$

where  $W\left(\frac{\lambda(\frac{1}{z+1})^{1/\beta}}{\beta}\right) e^{W\left(\frac{\lambda(\frac{1}{z+1})^{1/\beta}}{\beta}\right)} = \frac{\lambda(\frac{1}{z+1})^{1/\beta}}{\beta}$  and the deceleration parameter can be derived as

$$q(z) = \frac{1}{\beta \left( W\left(\frac{\lambda(\frac{1}{z+1})^{1/\beta}}{\beta}\right) + 1 \right)^2} - 1 \quad (17)$$

Both the Hubble and deceleration parameters are in the form of redshift. So, their parameters can be easily constrained by fitting them with various observational datasets.

### IV. OBSERVATIONAL DATA-DRIVEN ANALYSIS

This section highlights observational cosmology, which is crucial for the establishment of precise and coherent cosmological models. To accomplish this, it is important to constrain the model parameters, specifically  $\lambda$  and  $\beta$  through rigorous examination of observational data.

This investigation utilizes various observational datasets, including Hubble ( $H(z)$ ), Baryon Acoustic Oscillation (BAO) and Pantheon+SH0ES, to assess the validity of our chosen model. Through statistical analysis of these datasets, we find the best-fit model parameters and their associated confidence intervals, providing robust observational constraints on the model.

#### A. $H(z)$ Dataset

Early-type galaxies are used to estimate their differential evolutionary rates in order to obtain the Hubble parameter measurements. The Cosmic Chronometer (CC) strategy is the process by which these measurements are collected. The available data span a redshift range  $0.07 \leq z \leq 1.965$  [36–43]. The  $\chi^2$  estimation for this 32-point dataset can be calculated as

$$\chi_{H(z)}^2 = \sum_{i=1}^{32} \left[ \frac{(H_{\text{th}}(z_i, \theta) - H_{\text{obs}}(z_i))^2}{\sigma_H^2(z_i)} \right], \quad (18)$$

Here  $H_{\text{th}}(z_i, \theta)$  symbolises the theoretical Hubble parameter determined at redshift  $z_i$  for a specific collection of cosmological parameters  $\theta$ , while  $H_{\text{obs}}(z_i)$  reflects the associated observed values. The quantity  $\sigma_H^2(z_i)$  corresponds to the observational uncertainty related to the measured  $H_{\text{obs}}(z_i)$ .

## B. BAO Dataset

Baryon Acoustic Oscillations (BAO) are periodic fluctuations in the density of baryonic matter of the universe, resulting from acoustic density waves that transported primordial plasma of the early universe. These oscillations provide a unique mark on the matter power spectrum, and the location of the BAO peaks yield significant cosmological insights.

BAO peak measurements allow the estimation of the Hubble distance  $D_H(z)$  and the angular distance  $D_A(z)$ , enabling the constraint of parameters regarding DE. The acoustic horizon  $r$  determined by the BAO peaks, acts as a standard ruler that permits us to figure out both the redshift separation and the angular separation at a certain redshift  $z$ , defined as:  $\delta_z = r/D_H(z)$  and  $\delta_\theta = r/(1+z)D_A(z)$ . By adopting suitable assumptions for  $r$  and constraining the cosmological parameters that determine the ratios  $D_A(z)/r$  and  $D_H(z)/r$ , we may precisely calculate the Hubble parameter  $H(z)$ . This study employs 26 uncorrelated BAO radial measurements data points sourced from refs. [44–47, 47–53]. The  $\chi^2$  estimation for the BAO dataset is articulated as

$$\chi^2_{BAO}(\phi) = \sum_{i=1}^{26} \left[ \frac{(H_{th}(z_i, \phi) - H_{obs}(z_i))^2}{\sigma_H^2(z_i)} \right], \quad (19)$$

Here,  $H_{th}(z_i, \phi)$  implies the theoretical Hubble parameter at redshift  $z_i$  for a certain set of model parameters  $\phi$ ,  $H_{obs}(z_i)$  refers to the observed Hubble parameter derived from BAO observations, and  $\sigma_H(z_i)$  pertains to the observational uncertainties associated with the BAO data.

## C. Pantheon+SH0ES Dataset

Another baseline dataset employed in our MCMC analyses comprises observations from Type Ia supernova observations. These supernovae arise in binary star systems and play a key role in cosmology owing to their extremely uniform intrinsic luminosity, which lets them serve as reliable standard candles for the measurement of extragalactic distances. The distance modulus is defined as the difference between the measured apparent magnitude  $m$  and the absolute magnitude  $M$ , which characterizes the intrinsic luminosity of the source, and can be written as follows:

$$\mu(z_k) = m - M = 5 \log_{10}[D_L(z_k, \psi)] + 25 \quad (20)$$

where  $D_L(z_k, \psi)$  is the luminosity distance given by,

$$D_L(z_k, \psi) = c(1 + z_k) \int_0^{z_k} \frac{dz'}{H(z')} \quad (21)$$

Methodologically, the apparent magnitude of each Type Ia supernova is calibrated by adopting a fiducial absolute magnitude,  $M$ . Accordingly, within the MCMC framework,  $M$  is regarded as a nuisance parameter and marginalized. Theoretical cosmological models are employed to estimate the distance modulus for a chosen parameter space, which are then compared with the supernova measurements compiled in the Pantheon dataset. The cosmological parameters are constrained by minimizing a chi-square likelihood of the type [54],

$$\chi^2_{SN} = \Delta\mu^T C^{-1} \Delta\mu \quad (22)$$

where  $\Delta\mu = \mu_{th}(z_k, \psi) - \mu_{obs}(z_k)$ , and  $C$  is the covariance matrix incorporating both statistical and systematic uncertainties. Equivalently, we can express it as,

$$\chi^2(\psi) = \sum_{k=1}^N \sum_{l=1}^N [\mu_{th}(z_k, \psi) - \mu_{obs}(z_k)] (C^{-1})_{kl} \times [\mu_{th}(z_l, \psi) - \mu_{obs}(z_l)], \quad (23)$$

This study employs the Pantheon+SH0ES[55] dataset of type Ia supernovae, which is an updated and expanded version of the original pantheon sample. The original Pantheon compilation had 1048 SNIa with a redshift range up to  $z \sim 2.3$ , while the Pantheon+SH0ES collection has 1701 SNIa across an expanded redshift range  $0.001 < z < 2.25$ . The expanded coverage and addition of low-redshift supernovae facilitate a more rigorous analysis of systematic errors, providing enhanced precision in cosmological parameter constraints.

Upon separately examining the  $H(z)$ , BAO, and Pantheon+SH0ES datasets, we establish the optimal values of the model through a joint investigation by combining both the datasets. To accomplish this, we define the aggregated  $\chi^2$  function as the summation of the individual contributions from the observational Hubble parameter measurements  $H(z)$ , BAO, and Pantheon+SH0ES:

$$\chi_{total}^2 = \chi_{H(z)}^2 + \chi_{BAO}^2 + \chi_{SN}^2 \quad (24)$$

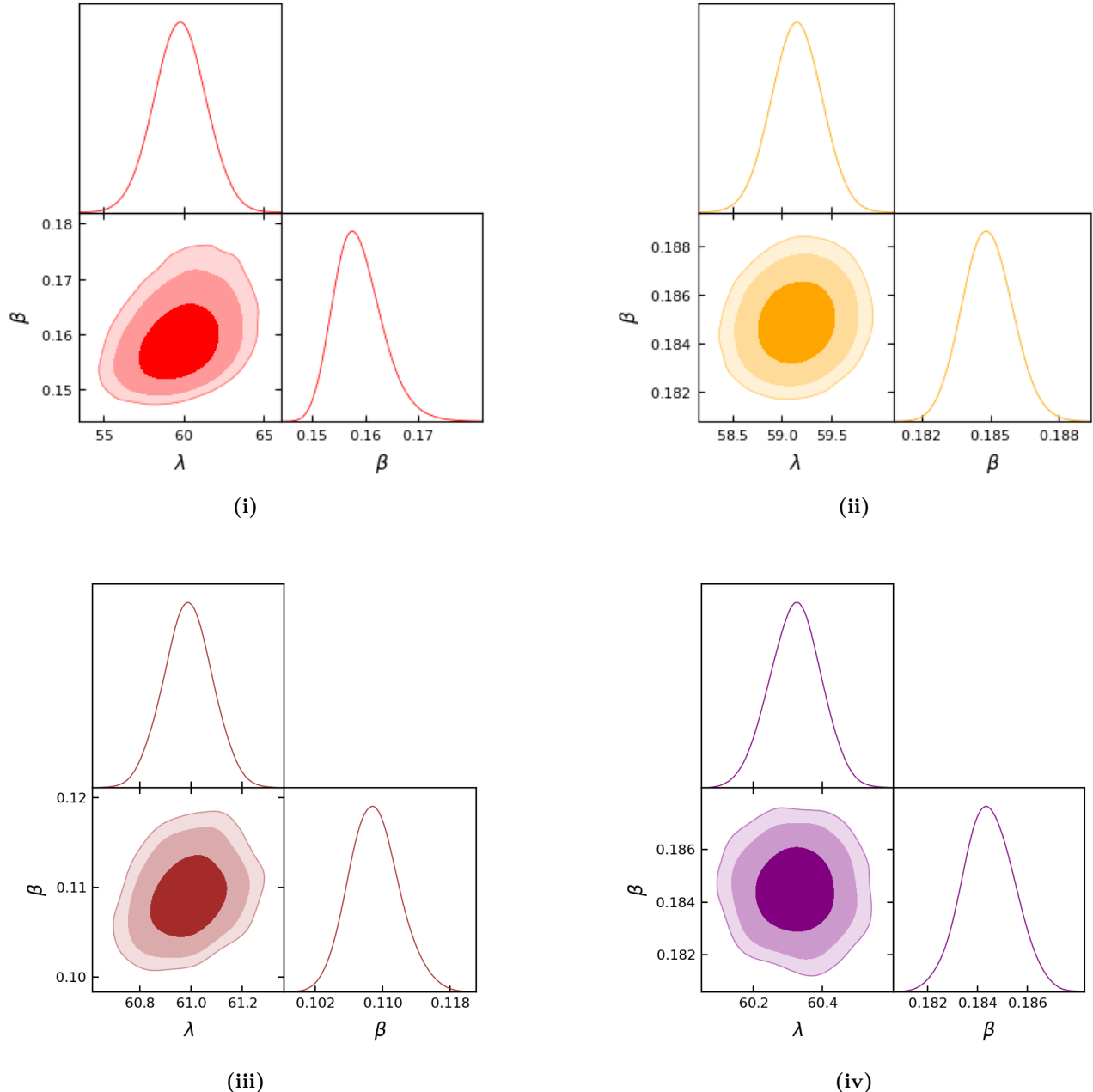


FIG. 1: 2D-contour plots generated from the analysis of (i)  $H(z)$ , (ii) BAO, (iii) Pantheon+SH0ES, and (iv) combined ( $H(z) + \text{BAO} + \text{Pantheon+SH0ES}$ ) datasets, illustrating the best-fit values and up to  $3\sigma$  confidence intervals for the model parameters  $\lambda$  and  $\beta$ .

The **Fig.1** represents the corner plots of the model parameters  $\lambda$  and  $\beta$  up to  $3\sigma$  confidence intervals extracted through MCMC approach by fitting the model with (i)  $H(z)$ , (ii) BAO, (iii) Pantheon+SH0ES and (iv) Combined datasets with the help of Bayesian statistics. In the **Table I**, the best-fit values of the model parameters with  $1\sigma$  (68% confidence),  $2\sigma$  (95% confidence), and  $3\sigma$  (99%) confidence intervals are presented and also, by considering these values we proceed further investigations. It is observed that the  $1\sigma$  values of  $\lambda$  and  $\beta$  are varying within the range around (59, 60) and (0.10, 0.19), presenting their tight constraints and reflecting the robustness of the hybrid scale factor.

Dataset		$\lambda$	$\beta$
Hubble	$1\sigma$	$59.7734^{+1.6081}_{-1.6041}$	$0.1584^{+0.005}_{-0.004}$
	$2\sigma$	$59.7734^{+3.1744}_{-3.1774}$	$0.1584^{+0.0108}_{-0.0074}$
	$3\sigma$	$59.7734^{+4.7788}_{-4.7729}$	$0.1584^{+0.0189}_{-0.0103}$
BAO	$1\sigma$	$59.1499^{+0.2534}_{-0.2541}$	$0.1849^{+0.0011}_{-0.0011}$
	$2\sigma$	$59.1499^{+0.4970}_{-0.5009}$	$0.1849^{+0.0022}_{-0.0021}$
	$3\sigma$	$59.1499^{+0.7501}_{-0.7593}$	$0.1849^{+0.0035}_{-0.0031}$
Pantheon+SH0ES	$1\sigma$	$60.9872^{+0.0957}_{-0.0931}$	$0.1090^{+0.0030}_{-0.0029}$
	$2\sigma$	$60.9872^{+0.1877}_{-0.1911}$	$0.1090^{+0.0063}_{-0.0056}$
	$3\sigma$	$60.9872^{+0.2938}_{-0.2869}$	$0.1090^{+0.0093}_{-0.0081}$
Combined	$1\sigma$	$60.3234^{+0.0724}_{-0.0771}$	$0.1844^{+0.0011}_{-0.0010}$
	$2\sigma$	$60.3234^{+0.1437}_{-0.1509}$	$0.1844^{+0.0021}_{-0.0021}$
	$3\sigma$	$60.3234^{+0.2191}_{-0.2132}$	$0.1844^{+0.0030}_{-0.0030}$

TABLE I: Parameter constraints for  $\lambda$  and  $\beta$ , exhibiting best-fit values with  $1\sigma$ ,  $2\sigma$ , and  $3\sigma$  confidence intervals derived from the  $H(z)$ , BAO, Pantheon+SH0ES and combined datasets.

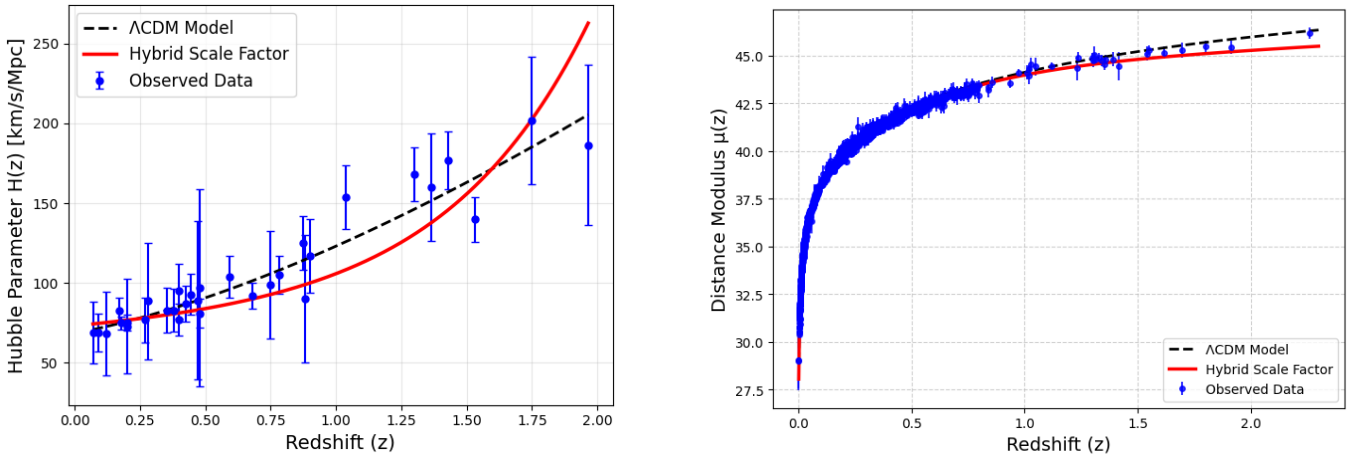


FIG. 2: The left panel illustrates the error bar plot of the Hubble parameter, whereas the right panel depicts the distance modulus function for the  $\Lambda$ CDM model and hybrid scale factor.

The left panel and right panel of **Fig.2** illustrates the error bar plot of the Hubble parameter and distance modulus function, respectively, showing that the Hubble model derived from the hybrid scale factor is greatly aligned with the  $\Lambda$ CDM model and observational data, with best-fit values of its parameters extracted through MCMC. The deceleration parameter presented in the **Fig.3** is staying negative throughout for the BAO and combined datasets, depicting the accelerating behaviour of the universe. The deceleration parameter transitions from positive values in

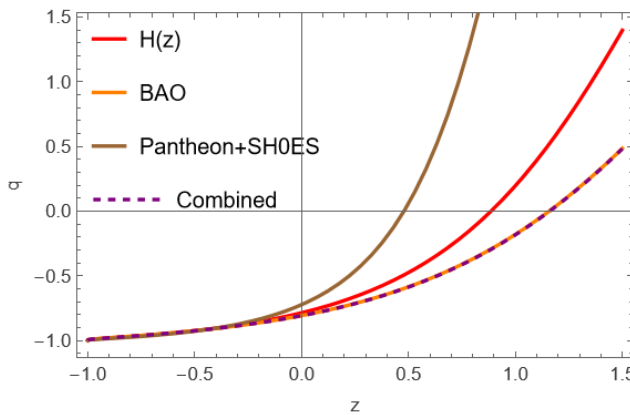


FIG. 3: Illustrates the plot of the deceleration parameter for  $H(z)$ , BAO, Pantheon+SH0ES, and combined datasets.

the early universe to  $q = -1$  at late times, denoting an evolution from a decelerated phase to an accelerated expansion for all considered datasets. Also, the values of  $q$  at the redshift  $z = 0$  are  $-0.79$ ,  $-0.81$ ,  $-0.73$ , and  $-0.81$  for  $H(z)$ , BAO, Pantheon+SH0ES and combined datasets and are in agreement with the literature [56–58].

## V. DYNAMICS IN RECONSTRUCTED $f(T)$ GRAVITY MODELS

$$\mathbf{A. Model I: } f(T) = T - \frac{a}{(-T/6)^n} + b(\frac{-T}{6})^m$$

Here, we propose a type of  $f(T)$  [59] theory analogous to the form of  $f(R) = R - \alpha/R^n + \beta R^m$  [60], mentioned as,

$$f(T) = T - \frac{a}{(-T/6)^n} + b(-T/6)^m \quad (25)$$

which appeared to be the novel combination of two forms  $\frac{a}{(-T/6)^n}$  [61] and  $b(\frac{-T}{6})^m$  [62]. Furthermore, when  $T \rightarrow \infty$ , GR is recovered if  $m \leq 1$  throughout early times; conversely, if  $m > 1$ , this specific  $f(T)$  theory diverges from GR even as  $T \rightarrow \infty$ . In later times, the term  $\frac{a}{(-T/6)^n}$  dominates and may cause accelerated expansion. The model form in (25) shows a linear behavior for  $n = 0$  and  $m = 1$ .

Consecutively, the first and second derivatives of the  $f(T)$  with respect to  $T$ , denoted as  $f_T$  and  $f_{TT}$  respectively, are determined and incorporated in equations (12) to (14). As a result, the equations reduced to;

$$\rho_{de} = \frac{1}{2} \left[ -12\tau \left( -\frac{1}{6}an(\tau)^{-n-1} - \frac{1}{6}bm(\tau)^{m-1} + 1 \right) + a(\tau)^{-n} - b(\tau)^m + 6\tau \right], \quad (26)$$

$$p_{de} = \frac{3\tau^2\gamma^2 (b(m-1)(2m-1)\tau^{m+n} - a(n+1)(2n+1))}{\gamma^2(an(2n+1) + \tau^n(12\lambda^2 - bm(2m-1)\tau^m)) + 12\lambda^2\tau^n + 24\lambda^2\gamma\tau^n}, \quad (27)$$

$$\begin{aligned} \omega_{de} = & \left( \frac{6\tau^2\gamma^2 (b(m-1)(2m-1)\tau^{m+n} - a(n+1)(2n+1))}{-12\tau \left( -\frac{1}{6}an\tau^{-n-1} - \frac{1}{6}bm\tau^{m-1} + 1 \right) + a\tau^{-n} - b\tau^m + 6\tau} \right) \\ & \times \left( \frac{1}{\gamma^2(an(2n+1) + \tau^n(12\lambda^2 - bm(2m-1)\tau^m)) + 12\lambda^2\tau^n + 24\lambda^2\gamma\tau^n} \right) \end{aligned} \quad (28)$$

where,  $\gamma = W\left(\frac{\lambda(\frac{1}{z+1})^{1/\beta}}{\beta}\right)$  and  $\tau = \left(\lambda + \frac{\lambda}{\gamma}\right)^2$ . Also,  $\rho_{de}$ ,  $p_{de}$ , and  $\omega$  represent the energy density, pressure, and EoS parameter for the DE sector.

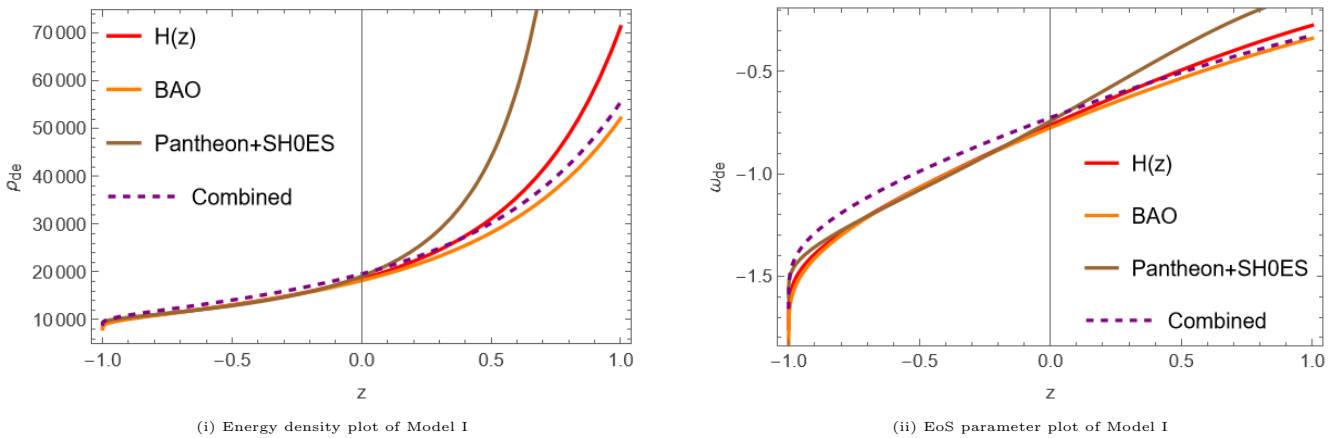


FIG. 4: The left panel displays energy density, and the right panel displays the EoS parameter plot of Model I for  $H(z)$ , BAO, Pantheon+SH0ES and combined datasets with the parameter scheme  $a = 0.665$ ,  $b = 0.084$ ,  $m = 1.505$ , and  $n = 0.245$ .

**Fig.4** illustrates the behaviors of energy density and EoS parameter of DE sector, depending upon the parameters  $\lambda$ ,  $\beta$ ,  $m$ ,  $n$ ,  $a$ , and  $b$ , where MCMC constrains the first two parameters, and the last three are selected to provide a

positive energy density. Throughout the plot, we get negative EoS parameter and stays in the quintessence region at the present time and the phantom model at the late-time for all observational datasets. The current values of the EoS parameter are around  $\omega_0 = -0.76$ ,  $\omega_0 = -0.78$ ,  $\omega_0 = -0.74$  and  $\omega_0 = -0.72$  for  $H(z)$ , BAO, Pantheon+SH0ES, and combined datasets respectively which are consistent with the refs.[63–65].

$$\mathbf{B. \ Model \ II:} \quad f(T) = T - aT_0 \left[ \left( 1 + \frac{T^2}{T_0^2} \right)^{-n} - 1 \right]$$

In analogous to a  $f(R)$  model proposed by Sato,  $f(R) = R + \alpha R_0 \left[ \left( 1 + \frac{R^2}{R_0^2} \right)^{-n} - 1 \right]$  [66], where  $\alpha, R_0$ , and  $n$  are positive constants and  $R_0$  is the order of the present Ricci scalar, here, we have proposed a form of  $f(T)$  [59]

$$f(T) = T - aT_0 \left[ \left( 1 + \frac{T^2}{T_0^2} \right)^{-n} - 1 \right] \quad (29)$$

where  $a, n$  are positive constants, and  $T_0$  is the order of the present Hubble parameter. This form reduces to a linear one in the absence of the constant  $n$ .

The rationale for this category of  $f(T)$  theories is created from their  $f(R)$  counterparts: firstly, the condition  $f(0) = 0$  ensures that in a flat spacetime, no cosmological constant appears, suggesting that the origin of DE is associated with geometry instead of a specific constant. Secondly, in both early and late cosmic epochs, such models emulate GR with a cosmological constant, but not a genuine constant; thereby, these theories can successfully undergo observational investigations and come out nearly indistinguishable from the  $\Lambda$ CDM model. Significantly, although  $\Lambda$ CDM struggles with the coincidence problem, these dynamic  $f(T)$  models, due to their evolving behaviour, can function equivalently to a cosmological constant, bypassing the coincidence issue entirely, rendering them highly appealing for further research.

Incorporating, the first and second derivatives of this  $f(T)$  form with respect to  $T$  (denoted as  $f_T$  and  $f_{TT}$ ) in equations (12) to (14), we get energy density, pressure and EoS parameter of the DE sector, respectively, as;

$$\rho_{de} = -6\tau \left( 1 - \frac{12an\tau\zeta^{-n-1}}{T_0} \right) + \frac{1}{2}aT_0 (\zeta^{-n} - 1) + 3\tau, \quad (30)$$

$$p_{de} = \frac{-6\tau \left( 1 - \frac{12an\tau\zeta^{-n-1}}{T_0} \right) + aT_0 (\zeta^{-n} - 1) - \frac{144an\tau^2(72(-n-1)\tau^2 + T_0^2\zeta)\zeta^{-n-2}}{T_0^3} + 6\tau}{2 \left( -\frac{36an\tau\zeta^{-n-1}}{T_0} - \frac{1728a(-n-1)n\tau^3\zeta^{-n-2}}{T_0^3} + 2 \right)}, \quad (31)$$

$$\omega_{de} = -\frac{-6\tau \left( 1 - \frac{12an\tau\zeta^{-n-1}}{T_0} \right) + aT_0 (\zeta^{-n} - 1) - \frac{144an\tau^2(72(-n-1)\tau^2 + T_0^2\zeta)\zeta^{-n-2}}{T_0^3} + 6\tau}{2 \left( -6\tau \left( 1 - \frac{12an\tau\zeta^{-n-1}}{T_0} \right) + \frac{1}{2}at (\zeta^{-n} - 1) + 3\tau \right) \left( -\frac{36an\tau\zeta^{-n-1}}{T_0} - \frac{1728a(-n-1)n\tau^3\zeta^{-n-2}}{T_0^3} + 2 \right)} \quad (32)$$

$$\text{where } \gamma = W \left( \frac{\lambda \left( \frac{1}{z+1} \right)^{1/\beta}}{\beta} \right), \tau = \left( \lambda + \frac{\lambda}{\gamma} \right)^2, \text{ and } \zeta = \left( \frac{36\tau^2}{T_0^2} + 1 \right).$$

In the **Fig.5**, the parameters  $\lambda, \beta, a$ , and  $n$  decide the behaviour of the energy density and the EoS parameter of the DE sector of which  $\lambda$  and  $\beta$  are constrained by the MCMC analysis, while  $a$  and  $n$  are chosen in such a manner to obtain the positive energy density. The EoS parameter stays negative throughout the plot and lies above  $-1$ , indicating the quintessence phase of DE. While the current values of  $\omega$  are around  $-0.619$  for all datasets, which are consistent with the literature [67? ].

$$\mathbf{C. \ Model \ III:} \quad f(T) = T + aT_0 \frac{(T^2/T_0^2)^n}{1 + (T^2/T_0^2)^n}$$

In this subsection, a function can be considered as [59]

$$f(T) = T + aT_0 \frac{(T^2/T_0^2)^n}{1 + (T^2/T_0^2)^n} \quad (33)$$

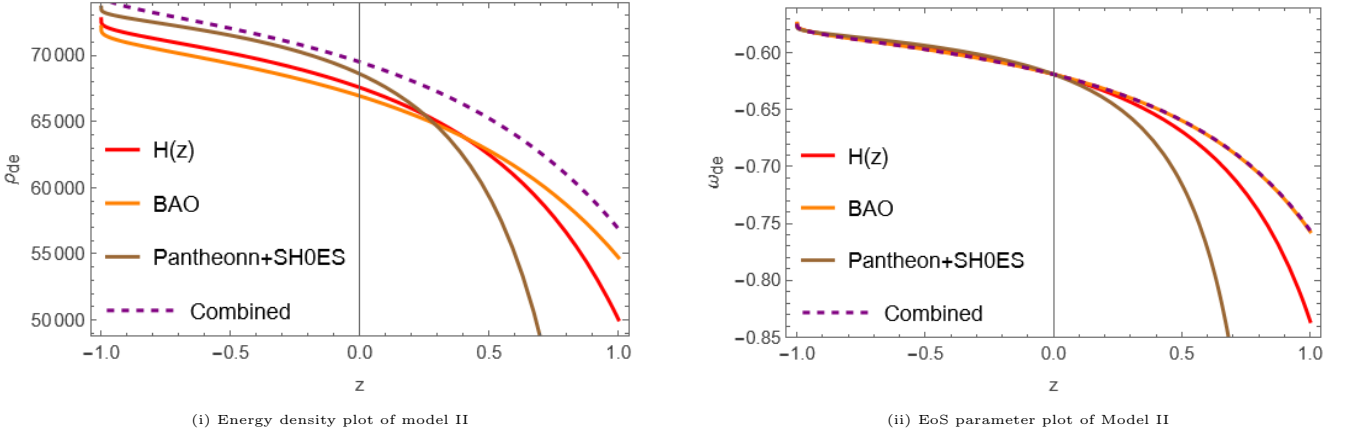


FIG. 5: The left panel displays energy density, and the right panel displays the EoS parameter plot of Model II for  $H(z)$ , BAO, Pantheon+SH0ES and combined datasets with the parameter scheme  $a = 5.2$  and  $n = 49.8$ .

This form is inspired by similar extensions in  $f(R)$  gravity,  $f(R) = R - \alpha R_0 \frac{(R^2/R_0^2)^n}{1+(R^2/R_0^2)^n}$  [68] that has been shown to align with both cosmological observations and local gravity tests. Also, this form reduces to linear form when the value of  $n$  vanishes.

Moreover, the explanation for embracing this form in  $f(T)$  gravity is threefold: Initially, at high redshift, the dynamics of the model closely align with the  $\Lambda$ CDM framework, offering it suitable for observational verification through cosmic microwave background (CMB) data. Secondly, at low redshift, it inherently triggers cosmic acceleration, demonstrating an expansion history akin to  $\Lambda$ CDM, but avoiding the necessity of a true cosmological constant. Third, it allows strictly regulated deviations from GR, incorporating  $\Lambda$ CDM as a specific instance, thereby enabling accurate cosmological constraints.

We, now, determine the derivatives of this  $f(T)$  form such as  $f_T$  and  $f_{TT}$  in order to replace their values in equations (12) to (14). Consequently, the reconstructed DE density, pressure and EoS parameter are obtained as;

$$\rho_{de} = \frac{a2^{2n+1}9^n n T_0 \left(\frac{\tau^2}{T_0^2}\right)^n}{\left(36^n \left(\frac{\tau^2}{T_0^2}\right)^n + 1\right)^2} + \frac{1}{2} a T_0 \left( \frac{1}{36^n \left(\frac{\tau^2}{T_0^2}\right)^n + 1} - 1 \right) - 3\tau \quad (34)$$

$$p_{de} = \frac{a\tau^2 3^{2n+1} t(\gamma)^2 \Theta \left(\frac{\tau^2}{t^2}\right)^n}{2 \left( 9^n \left(\frac{\tau^2}{t^2}\right)^n \Xi + 324^n \left(\frac{\tau^2}{t^2}\right)^{2n} \Upsilon + \tau^2 2^{4n+1} 3^{6n+1} (\gamma)^2 \left(\frac{\tau^2}{t^2}\right)^{3n} + 3\tau^2 2^{1-2n} (\gamma)^2 \right)} \quad (35)$$

$$\begin{aligned} \omega_{de} = & \frac{a\tau^2 3^{2n+1} t \gamma^2 \Theta \left(\frac{\tau^2}{t^2}\right)^n}{2 \left( \frac{a 2^{2n+1} 9^n n t \left(\frac{\tau^2}{t^2}\right)^n}{\left(36^n \left(\frac{\tau^2}{t^2}\right)^n + 1\right)^2} + \frac{1}{2} a t \left( \frac{1}{36^n \left(\frac{\tau^2}{t^2}\right)^n + 1} - 1 \right) - 3\tau \right)} \\ & \times \frac{1}{9^n \left(\frac{\tau^2}{t^2}\right)^n \Xi + 324^n \left(\frac{\tau^2}{t^2}\right)^{2n} \Upsilon + \tau^2 2^{4n+1} 3^{6n+1} \gamma^2 \left(\frac{\tau^2}{t^2}\right)^{3n} + 3\tau^2 2^{1-2n} \gamma^2} \quad (36) \end{aligned}$$

where  $\gamma = W \left( \frac{\lambda \left(\frac{1}{z+1}\right)^{1/\beta}}{\beta} \right)$ ,  $\tau = \left( \lambda + \frac{\lambda}{\gamma} \right)^2$ ,  $\Theta = \left( 8n^2 - 2^{2n+1} 9^n (n+1) (4n-1) \left(\frac{\tau^2}{t^2}\right)^n + 1296^n \left(\frac{\tau^2}{t^2}\right)^{2n} - 6n + 1 \right)$ ,  $\Xi = ((an(1-4n)t + 18\lambda^2) \gamma^2 + 18\lambda^2 + 36\lambda^2\gamma)$ , and  $\Upsilon = ((an(4n+1)t + 18\lambda^2) \gamma^2 + 18\lambda^2 + 36\lambda^2\gamma)$ .

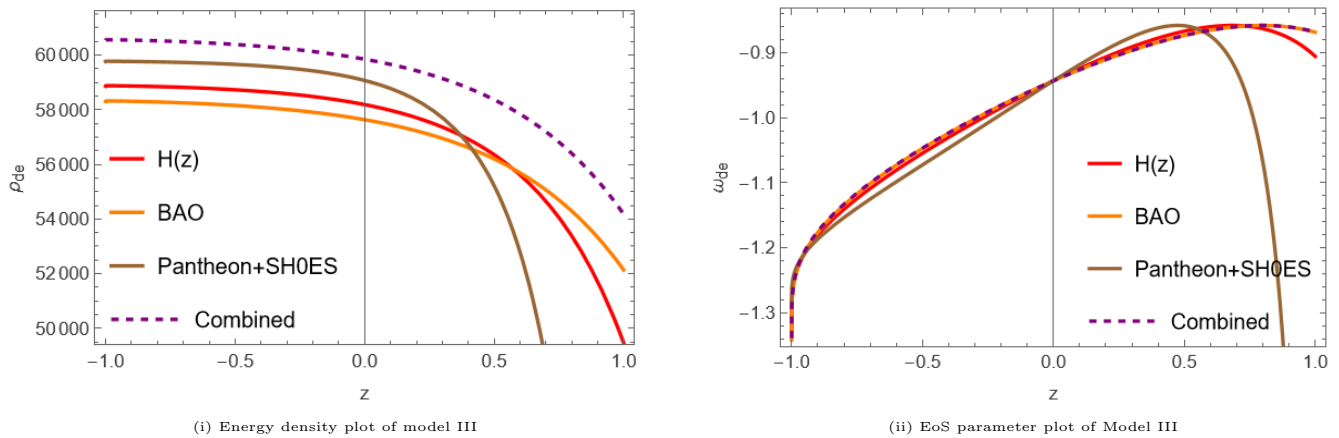


FIG. 6: The left panel displays energy density, and the right panel displays the EoS parameter plot of Model III for  $H(z)$ , BAO, Pantheon+SH0ES and combined datasets with the parameter scheme  $a = 12.15$  and  $n = 0.15$ .

The expressions present in equations (34) and (36) can be graphically analysed for different datasets because they are dependent upon the Hubble parameter derived from the hybrid scale factor. We can see in Fig.6 that the energy density of the DE sector for Model III remains positive throughout, driven by the parameters  $\lambda$ ,  $\beta$ ,  $m$ , and  $n$  for the three data sets, satisfying the accelerated expansion nature of the universe. Also, the EoS parameter remains negative for all the datasets, indicating the quintessence region at present time and phantom phase at the late time. We can follow the literature [57, 65] with which the current values of the EoS parameter around  $\omega_0 = -0.944$ ,  $\omega_0 = -0.943$ ,  $\omega_0 = -0.945$ , and  $\omega_0 = -0.944$  for  $H(z)$ , BAO, Pantheon+SH0ES, and combined datasets, respectively, are consistent.

Based on the results of three above functional forms, a comparison table can be given as

Parameter	Model I				Model II				Model III			
	$H(z)$	BAO	Pantheon+SH0ES	Combined	$H(z)$	BAO	Pantheon+SH0ES	Combined	$H(z)$	BAO	Pantheon+SH0ES	Combined
$H(z_0)$ Km s $^{-1}$ Mpc $^{-1}$	73.2296	72.8813	73.7845	74.2685	73.2296	72.8813	73.7845	74.2685	73.2296	72.8813	73.7845	74.2685
$q(z_0)$	-0.79	-0.809	-0.73	-0.805	-0.79	-0.809	-0.73	-0.805	-0.79	-0.809	-0.73	-0.805
$\omega(z_0)$	-0.76	-0.78	-0.74	-0.72	-0.619	-0.619	-0.619	-0.619	-0.944	-0.943	-0.945	-0.944

TABLE II: Comparison of parameters for Model I, Model II, and Model III using different datasets.

The results presented in the table indicate that, at the present epoch ( $z=0$ ), the equation-of-state (EoS) parameter for all three reconstructed models resides within the quintessence regime, regardless of their distinct evolutionary trajectories at other redshifts. Furthermore, the present-day values of the Hubble parameter and the deceleration parameter are independent of the specific model construction. Consequently, these quantities attain identical values across all three proposed  $f(T)$  formulations at zero redshift.

## VI. ENERGY CONDITIONS

For further analysis, in this section, we investigate the behaviour of the energy conditions. The energy conditions are essential concepts for understanding the behaviour of geodesics in the universe, derivable from the Raychaudhuri equations and can be represented as

- **Null Energy Condition (NEC):**  $\rho + p \geq 0$ ;
- **Weak Energy Condition (WEC):**  $\rho \geq 0$  and  $\rho + p \geq 0$ ;
- **Strong Energy Condition (SEC):**  $\rho + 3p \geq 0$ ;
- **Dominant Energy Condition (DEC):**  $\rho - p \geq 0$

Examining energy conditions enables for an understanding of the characteristics of matter and energy in the universe, an essential step in comprehending its accelerated expansion and the impact of DE. Energy conditions fundamentally serve as boundary restrictions that regulate the evolution of the cosmos [69]. Moreover, due to the fundamental causal structure of spacetime, gravitational interactions are fundamentally shaped by energy conditions [70].

Fig.7 exhibits the behaviour of the energy conditions for Model I for  $H(z)$ , BAO, Pantheon+SH0ES and combination of all. For all three datasets, NEC and DEC are getting almost satisfied everywhere, but SEC is getting violated

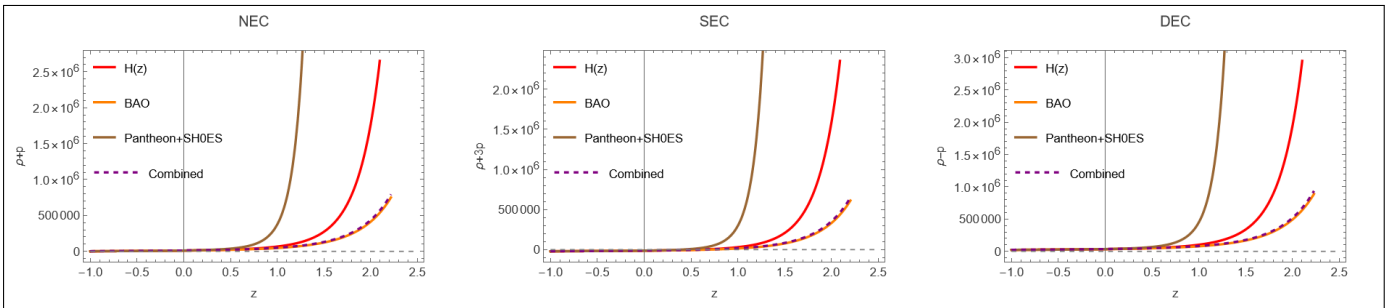


FIG. 7: Energy conditions versus redshift for Model I over  $H(z)$ , BAO, Pantheon+SH0ES and combined datasets with the parameter scheme  $a = 0.665$ ,  $b = 0.084$ ,  $m = 1.505$ , and  $n = 0.245$ .

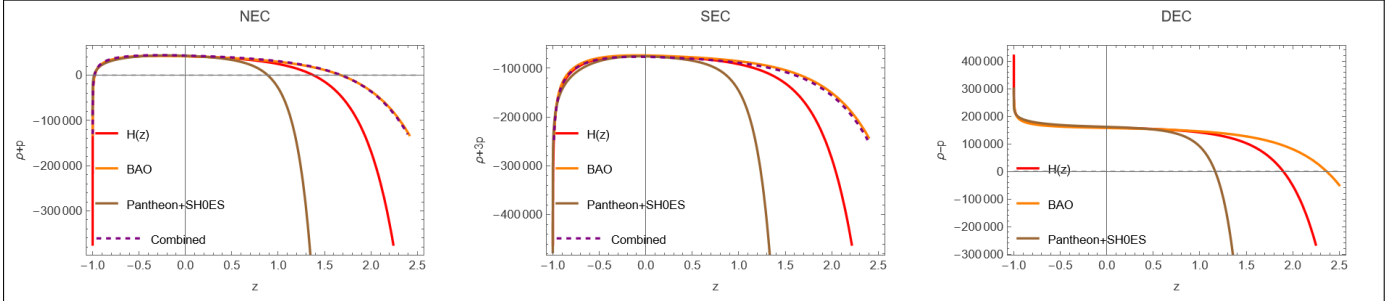


FIG. 8: Energy conditions versus redshift for Model II over  $H(z)$ , BAO, Pantheon+SH0ES and combined datasets with the parameter scheme  $a = 5.2$  and  $n = 49.8$ .

in the redshift range around  $[-1, 0.55]$ ,  $[-1, 0.65]$ ,  $[-1, 0.38]$ , and  $[-1, 0.60]$  for  $H(z)$ , BAO, Pantheon+SH0ES and combined datasets, respectively, which reflects the accelerated expansion at the current epoch and late-time. The energy conditions of Model II in **Fig.8** illustrates: (i) the satisfaction of NEC in the redshift range around  $(-0.98, 1.37)$ ,  $(-0.98, 1.68)$ ,  $(-0.98, 0.88)$ , and  $(-0.98, 1.69)$  for  $H(z)$ , BAO, Pantheon+SH0ES and combined datasets, respectively, (ii) satisfaction of DEC in the redshift range around  $[-1, 1.90]$ ,  $[-1, 2.36]$ ,  $[-1, 1.16]$ , and  $[-1, 2.37]$  for  $H(z)$ , BAO, Pantheon+SH0ES and combination of all respectively, and especially (iii) the violation of SEC throughout the plot for all the three datasets, reflecting the expansion of the universe in an accelerated manner. The behaviour of the energy conditions in **Fig.9** demonstrates the accelerated expansion of the cosmos exhibiting the violating behaviour of SEC throughout the plot for all the datasets, satisfaction of NEC in the redshift range around  $(-0.98, 1.18)$ ,  $(-0.98, 1.42)$ ,  $(-0.99, 0.78)$ , and  $(-0.98, 1.43)$  for  $H(z)$ , BAO, Pantheon+SH0ES and combined datasets and also the satisfaction of DEC in the redshift range around  $[-1, 1.83]$ ,  $[-1, 2.27]$ ,  $[-1, 1.13]$ , and  $[-1, 2.27]$  for  $H(z)$ , BAO, Pantheon+SH0ES and combined data.

## VII. CONCLUSION

In the present work, we reconstruct  $f(T)$  gravity by examining three distinct functional forms of  $f(T)$  and solving the corresponding modified field equations within the Friedmann–Lemaître–Robertson–Walker (FLRW) cosmological framework. The cosmic expansion is modeled through a hybrid scale factor that incorporates both power-law and exponential behaviors. The free parameters associated with this hybrid parametrization are constrained using a Markov Chain Monte Carlo (MCMC) analysis under the framework of Bayesian Statistics and

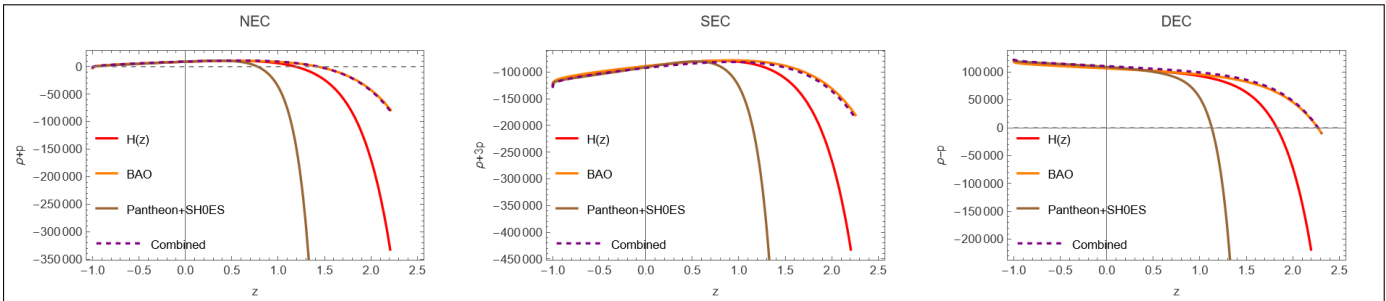


FIG. 9: Energy conditions versus redshift for Model III over  $H(z)$ , BAO, Pantheon+SH0ES and combined datasets with the parameter scheme  $a = 12.15$  and  $n = 0.15$ .

applied to multiple observational datasets, such as;  $H(z)$ , BAO, Pantheon+SH0ES, and their joint compilation. By confronting the theoretical predictions with observational evidence, we obtain bounds on the model parameters and verify that the reconstructed scenarios provide an adequate description of the Universe's dynamical evolution. This approach contributes to a deeper understanding of the expansion history and underlying properties of the cosmos.

This analysis leads to several noteworthy results,

- The proposed hybrid scale factor exhibits strong agreement with the standard  $\Lambda$ CDM scenario and observational data, as evidenced by the Hubble and distance modulus analyses. By combining power-law and exponential terms, it successfully captures the transition from an early inflationary regime to a late-time accelerated phase. The present epoch behavior closely mimics that of the concordance  $\Lambda$ CDM model. Observational indications of late-time acceleration imply a transition from an earlier decelerating phase to the current accelerating phase, characterized by a signature change in the deceleration parameter. Unlike pure power law or exponential scale factors, which typically yield constant deceleration parameters and are therefore less suitable for modeling cosmic speed-up, the hybrid form effectively reproduces a dynamically evolving deceleration parameter with positive values at early times and negative values at late times.
- The deceleration parameter, for all considered datasets, stays negative at present and late-time but shows a transition from deceleration to acceleration phase in the early universe. The transition from deceleration to acceleration for Hubble, BAO, Pantheon+SH0ES and combined dataset shows the value  $z_t = 0.89$ ,  $z_t = 1.16$ ,  $z_t = 0.48$  and  $z_t = 1.16$  respectively. The present value of the deceleration parameter has been obtained as  $q_0 = -0.79$ ,  $q_0 = 0.81$ ,  $q_0 = 0.73$  and  $q_0 = 0.81$  in the similar fashion which indicates the current acceleration nature of the universe [57, 58, 71].
- The energy density of the DE sector for all three models remains positive throughout the plot, ensuring the physical viability of the reconstructed scenarios.
- According to the results presented in Table II, the equation-of-state (EoS) parameter for Models I and II evolves from a quintessence-like regime at present to a phantom regime at late times across all datasets. In contrast, Model I consistently remains within the quintessence region at both present and late epochs. Moreover, the current values of the EoS parameter are in good agreement with previously reported results in the literature [57, 63–65, 67? ].
- To assess the viability of the modified gravity framework, the standard energy conditions; namely, the null energy condition (NEC) and dominant energy condition (DEC) are examined. Depending on the redshift interval and model considered, these conditions may be either satisfied or violated. The strong energy condition (SEC) is violated near the present epoch for Model I and throughout the evolution for Models II and III across all datasets.

In conclusion, the present work provides a comprehensive analysis of late-time cosmological evolution within the framework of non-linear  $f(T)$  gravity. The key geometrical and dynamical quantities are estimated using a Bayesian statistical framework, ensuring robust parameter inference. For all three reconstructed models, the obtained parameter values exhibit strong consistency with recent high-precision satellite observations. Future investigations, particularly those involving dynamical stability assessments and the inclusion of more recent observational datasets, would further enhance the reliability and scope of the proposed models.

## VIII. REFERENCES

---

- [1] A.G. Riess, A.V. Filippenko, P. Challis, A. Clocchiatti, A. Diercks, P.M. Garnavich et al., *Observational evidence from supernovae for an accelerating universe and a cosmological constant*, *Astron. J.* **116** (1998) 1009.
- [2] S. Perlmutter, G. Aldering, G. Goldhaber, R.A. Knop, P. Nugent, P.G. Castro et al., *Measurements of  $\omega$  and  $\lambda$  from 42 high-redshift supernovae*, *Astrophys. J.* **517** (1999) 565.
- [3] D.N. Spergel, R. Bean, O. Doré, M.R. Nolta, C.L. Bennett, J. Dunkley et al., *Three-year wilkinson microwave anisotropy probe (wmap) observations: Implications for cosmology*, *Astrophys. J. Suppl.* **170** (2007) 377 [[astro-ph/0603449](#)].
- [4] E. Komatsu, J. Dunkley, M.R. Nolta, C.L. Bennett, B. Gold, G. Hinshaw et al., *Five-year wilkinson microwave anisotropy probe (wmap) observations: Cosmological interpretation*, *Astrophys. J. Suppl.* **180** (2009) 330 [[0803.0547](#)].
- [5] D.J. Eisenstein, I. Zehavi, D.W. Hogg, R. Scoccimarro, M.R. Blanton, R.C. Nichol et al., *Detection of the baryon acoustic peak in the large-scale correlation function of SDSS luminous red galaxies*, *Astrophys. J.* **633** (2005) 560 [[astro-ph/0501171](#)].
- [6] W.J. Percival, B.A. Reid, D.J. Eisenstein, N.A. Bahcall, T. Budavari, J.A. Frieman et al., *Baryon acoustic oscillations in the SDSS data release 7 (DR7) galaxy sample*, *Mon. Not. Roy. Astron. Soc.* **401** (2010) 2148 [[0907.1660](#)].

[7] D.H. Weinberg, M.J. Mortonson, D.J. Eisenstein, C. Hirata, A.G. Riess and E. Rozo, *Observational probes of cosmic acceleration*, *Phys. Rept.* **530** (2013) 87 [[1201.2434](#)].

[8] S. Nojiri and S.D. Odintsov, *Introduction to modified gravity and gravitational alternative for dark energy*, *Int. J. Geom. Meth. Mod. Phys.* **4** (2007) 115 [[hep-th/0601213](#)].

[9] A.G. Riess, S. Casertano, W. Yuan, L.M. Macri and D. Scolnic, *Large magellanic cloud cepheid standards provide a 1% foundation for the determination of the hubble constant and stronger evidence for physics beyond  $\Lambda$ cdm*, *Astrophys. J.* **876** (2019) 85 [[1903.07603](#)].

[10] A. Nájera and A. Fajardo, *Fitting  $f(Q, T)$  gravity models with a  $\lambda$ CDM limit using  $H(z)$  and pantheon data*, *Phys. Dark Univ.* **34** (2021) 100889 [[2104.XXXX](#)].

[11] E.L.B. Junior, M.E. Rodrigues, I.G. Salako and M.J.S. Houndjo, *Reconstruction, thermodynamics and stability of the  $\lambda$ CDM model in  $f(T, T)$  gravity*, *Class. Quant. Grav.* **33** (2016) 125006 [[1501.00621](#)].

[12] A. Raichoor, A. de Mattia, A.J. Ross, C. Zhao, S. Alam, S. Avila et al., *The completed SDSS-IV extended baryon oscillation spectroscopic survey: Large-scale structure catalogues and measurement of the isotropic BAO between redshift 0.6 and 1.1 for the emission line galaxy sample*, *Mon. Not. Roy. Astron. Soc.* **500** (2020) 3254 [[2007.09000](#)].

[13] R.-G. Cai and A. Wang, *Cosmology with interaction between phantom dark energy and dark matter and the coincidence problem*, *JCAP* **2005** (2005) 002 [[hep-th/0411025](#)].

[14] S. Weinberg, *The cosmological constant problem*, *Rev. Mod. Phys.* **61** (1989) 1.

[15] T.P. Sotiriou and V. Faraoni,  *$f(R)$  theories of gravity*, *Rev. Mod. Phys.* **82** (2010) 451 [[0805.1726](#)].

[16] J.B. Jiménez, L. Heisenberg and T. Koivisto, *Coincident general relativity*, *Phys. Rev. D* **98** (2018) 044048 [[1710.03116](#)].

[17] D. Rovere, *Covariant fractons and weitzenböck torsion*, [2505.21022](#).

[18] K. Hayashi and T. Shirafuji, *New general relativity*, *Phys. Rev. D* **19** (1979) 3524.

[19] C. Pellegrini and J. Plebanski, *Tetrad fields and gravitational fields*, *Kgl. Danske Videnskab. Selskab, Mat. Fys. Skr.* **2** (1962) 1.

[20] N. Tamanini and C.G. Böhmer, *Good and bad tetrads in  $f(T)$  gravity*, *Phys. Rev. D* **86** (2012) 044009 [[1204.4593](#)].

[21] K. Bamba and C.-Q. Geng, *Thermodynamics of cosmological horizons in  $f(T)$  gravity*, *JCAP* **2011** (2011) 008 [[1109.1694](#)].

[22] S.-H. Chen, J.B. Dent, S. Dutta and E.N. Saridakis, *Cosmological perturbations in  $f(T)$  gravity*, *Phys. Rev. D* **83** (2011) 023508 [[1008.1250](#)].

[23] S. Capozziello, P.A. González, E.N. Saridakis and Y. Vásquez, *Exact charged black-hole solutions in  $d$ -dimensional  $f(T)$  gravity: Torsion vs curvature analysis*, *JHEP* **2013** (2013) 039 [[1210.1098](#)].

[24] C.-Q. Geng, C.-C. Lee and E.N. Saridakis, *Observational constraints on teleparallel dark energy*, *JCAP* **2012** (2012) 002 [[1110.0913](#)].

[25] B. Li, T.P. Sotiriou and J.D. Barrow, *Large-scale structure in  $f(T)$  gravity*, *Phys. Rev. D* **83** (2011) 104017 [[1103.2786](#)].

[26] L.K. Duchaniya, S.V. Lohakare, B. Mishra and S.K. Tripathy, *Dynamical stability analysis of accelerating  $f(T)$  gravity models*, *Eur. Phys. J. C* **82** (2022) 465 [[2204.XXXX](#)].

[27] K. Bamba, R. Myrzakulov, S. Nojiri and S.D. Odintsov, *Reconstruction of  $f(T)$  gravity: Rip cosmology, finite-time future singularities, and thermodynamics*, *Phys. Rev. D* **85** (2012) 104036 [[1202.4057](#)].

[28] K. Bamba, S. Capozziello, S. Nojiri and S.D. Odintsov, *Dark energy cosmology: the equivalent description via different theoretical models and cosmography tests*, *Astrophysics and Space Science* **342** (2012) 155–228.

[29] B. Mishra and S.K. Tripathy, *Anisotropic dark energy model with a hybrid scale factor*, *Mod. Phys. Lett. A* **30** (2015) 1550175.

[30] B. Mishra, P.K. Sahoo and P.P. Ray, *Accelerating dark energy cosmological model in two fluids with hybrid scale factor*, *Int. J. Geom. Meth. Mod. Phys.* **14** (2017) 1750124.

[31] B. Mishra, P.P. Ray and S.K.J. Pacif, *Dark energy cosmological models with general forms of scale factor*, *Eur. Phys. J. Plus* **132** (2017) 1697.

[32] B. Mishra, S.K. Tripathy and S. Tarai, *Cosmological models with a hybrid scale factor in an extended gravity theory*, *Mod. Phys. Lett. A* **33** (2018) 1850052.

[33] A. Einstein, *Riemann-geometrie mit aufrechterhaltung des begriffes des fernparallelismus*, *Sitzungsber. Preuss. Akad. Wiss. Berlin (Math. Phys.)* (1928) 217.

[34] R. Aldrovandi and J.G. Pereira, *Teleparallel Gravity: An Introduction*, Springer (2012).

[35] F.K. Anagnostopoulos, S. Basilakos and E.N. Saridakis, *Bayesian analysis of  $f(T)$  gravity using  $f\sigma_8$  data*, *Phys. Rev. D* **100** (2019) 083517 [[1907.07533](#)].

[36] C. Zhang, H. Zhang, S. Yuan, S. Liu, T.-J. Zhang and Y.-C. Sun, *Four new observational  $H(z)$  data from luminous red galaxies in the SDSS data release seven*, *Res. Astron. Astrophys.* **14** (2014) 1221 [[1207.4541](#)].

[37] J. Simon, L. Verde and R. Jimenez, *Constraints on the redshift dependence of the dark energy potential*, *Phys. Rev. D* **71** (2005) 123001 [[astro-ph/0412269](#)].

[38] M. Moresco, A. Cimatti, R. Jimenez, L. Pozzetti, G. Zamorani, M. Bolzonella et al., *Improved constraints on the expansion rate of the universe up to  $z \sim 1.1$  from the spectroscopic evolution of cosmic chronometers*, *JCAP* **2012** (2012) 006 [[1201.3609](#)].

[39] M. Moresco, L. Pozzetti, A. Cimatti, R. Jimenez, C. Maraston, L. Verde et al., *A 6% measurement of the hubble parameter at  $z \sim 0.45$ : Direct evidence of the epoch of cosmic re-acceleration*, *JCAP* **2016** (2016) 014 [[1601.01701](#)].

[40] D. Stern, R. Jimenez, L. Verde, M. Kamionkowski and S.A. Stanford, *Cosmic chronometers: Constraining the equation of state of dark energy. i:  $H(z)$  measurements*, *JCAP* **2010** (2010) 008 [[0907.3149](#)].

[41] A.L. Ratsimbazafy, S.I. Loubser, S.M. Crawford, C.M. Cress, B.A. Bassett, R.C. Nichol et al., *Age-dating luminous red galaxies observed with the southern african large telescope*, *Mon. Not. Roy. Astron. Soc.* **467** (2017) 3239 [[1702.00418](#)].

[42] M. Moresco, *Raising the bar: New constraints on the hubble parameter with cosmic chronometers at  $z \sim 2$* , *Mon. Not. Roy. Astron. Soc. Lett.* **450** (2015) L16 [[1503.01116](#)].

[43] N. Borghi, M. Moresco and A. Cimatti, *Toward a better understanding of cosmic chronometers: A new measurement of*

$H(z)$  at  $z \sim 0.7$ , *Astrophys. J. Lett.* **928** (2022) L4 [[2111.XXXXX](#)].

[44] E.G. naga, A. Cabré and L. Hui, *Clustering of luminous red galaxies – iv. baryon acoustic peak in the line-of-sight direction and a direct measurement of  $H(z)$* , *Mon. Not. Roy. Astron. Soc.* **399** (2009) 1663 [[0807.3551](#)].

[45] C.-H. Chuang and Y. Wang, *Modelling the anisotropic two-point galaxy correlation function on small scales and single-probe measurements of  $H(z)$ ,  $d_a(z)$  and  $f(z)\sigma_8(z)$  from the SDSS DR7 luminous red galaxies*, *Mon. Not. Roy. Astron. Soc.* **435** (2013) 255 [[1209.0210](#)].

[46] S. Alam, M. Ata, S. Bailey, F. Beutler, D. Bizyaev, J.A. Blazek et al., *The clustering of galaxies in the completed SDSS-III baryon oscillation spectroscopic survey: Cosmological analysis of the DR12 galaxy sample*, *Mon. Not. Roy. Astron. Soc.* **470** (2017) 2617 [[1607.03155](#)].

[47] L. Anderson, E. Aubourg, S. Bailey, F. Beutler, V. Bhardwaj, M. Blanton et al., *The clustering of galaxies in the SDSS-III baryon oscillation spectroscopic survey: Baryon acoustic oscillations in the data releases DR10 and DR11 galaxy samples*, *Mon. Not. Roy. Astron. Soc.* **441** (2014) 24 [[1312.4877](#)].

[48] Y. Wang, G.-B. Zhao, C.-H. Chuang, A.J. Ross, W.J. Percival, H. Gil-Marín et al., *The clustering of galaxies in the completed SDSS-III baryon oscillation spectroscopic survey: Tomographic BAO analysis of DR12 combined sample in configuration space*, *Mon. Not. Roy. Astron. Soc.* **469** (2017) 3762 [[1703.02836](#)].

[49] T. Delubac, J.E. Bautista, N.G. Busca, J. Rich, D. Kirkby, S. Bailey et al., *Baryon acoustic oscillations in the Ly $\alpha$  forest of BOSS DR11 quasars*, *Astron. Astrophys.* **574** (2015) A59 [[1404.1801](#)].

[50] A. Oka, S. Saito, T. Nishimichi, A. Taruya and K. Yamamoto, *Simultaneous constraints on the growth of structure and cosmic expansion from the multipole power spectra of the SDSS DR7 LRG sample*, *Mon. Not. Roy. Astron. Soc.* **439** (2014) 2515 [[1310.2820](#)].

[51] C. Blake, S. Brough, M. Colless, C. Contreras, W. Couch, S. Croom et al., *The wigglez dark energy survey: Joint measurements of the expansion and growth history at  $z < 1$* , *Mon. Not. Roy. Astron. Soc.* **425** (2012) 405 [[1204.3674](#)].

[52] N.G. Busca et al., *Baryon acoustic oscillations in the Ly $\alpha$  forest of BOSS quasars*, *Astron. Astrophys.* **552** (2013) A96 [[1211.2616](#)].

[53] J.E. Bautista, N.G. Busca, J. Guy, J. Rich, M. Blomqvist, H. du Mas des Bourboux et al., *Measurement of baryon acoustic oscillation correlations at  $z = 2.3$  with SDSS DR12 Ly $\alpha$ -Forests*, *Astron. & Astrophys.* **603** (2017) A12 [[1702.00176](#)].

[54] A. Conley, J. Guy, M. Sullivan, N. Regnault, P. Astier, C. Balland et al., *Supernova constraints and systematic uncertainties from the first three years of the supernova legacy survey*, *Astrophys. J. Suppl. Ser.* **192** (2011) 1.

[55] D. Scolnic, D. Brout, A. Carr, A.G. Riess, T.M. Davis, A. Dwomoh et al., *The pantheon+ analysis: the full data set and light-curve release*, *Astrophys. J.* **938** (2022) 113.

[56] D. Camarena and V. Marra, *Local determination of the hubble constant and the deceleration parameter*, *Phys. Rev. Res.* **2** (2020) 013028.

[57] S.A. Kadam, B. Mishra and S.K. Tripathy, *Dynamical features of  $f(T,B)$  cosmology*, *Mod. Phys. Lett. A* **37** (2022) 2250104.

[58] S. Mandal, S. Pradhan, P.K. Sahoo and T. Harko, *Cosmological observational constraints on the power-law  $f(Q)$  type modified gravity theory*, *Eur. Phys. J. C* **83** (2023) 12339.

[59] R.-J. Yang, *New types of  $f(T)$  gravity*, *Eur. Phys. J. C* **71** (2011) 1797.

[60] S. Nojiri and S.D. Odintsov, *Modified gravity with negative and positive powers of curvature: Unification of inflation and cosmic acceleration*, *Phys. Rev. D* **68** (2003) 123512.

[61] G.R. Bengochea and R. Ferraro, *Dark torsion as the cosmic speed-up*, *Phys. Rev. D* **79** (2009) 124019.

[62] E.V. Linder, *Einstein's other gravity and the acceleration of the universe*, *Phys. Rev. D* **81** (2010) 127301.

[63] M. Koussour, N.S. Kavya, V. Venkatesha and N. Myrzakulov, *Cosmic expansion beyond  $\lambda$ CDM: Investigating power-law and logarithmic corrections*, *Eur. Phys. J. Plus* **139** (2024) 4955.

[64] N. Myrzakulov, M. Koussour and D.J. Gogoi, *A new  $Om(z)$  diagnostic of dark energy in general relativity theory*, *Eur. Phys. J. C* **83** (2023) 11794.

[65] Planck Collaboration, *Planck 2018 results. i. overview and the cosmological legacy of planck*, *Astron. Astrophys.* **641** (2020) A1.

[66] A.A. Starobinsky, *Disappearing cosmological constant in  $f(R)$  gravity*, *JETP Lett.* **86** (2007) 157.

[67] R. Bhagat, S.K. Tripathy and B. Mishra, *Logarithmic and strong coupling models in weyl-type  $f(Q,T)$  gravity*, 2025.

[68] W. Hu and I. Sawicki, *Models of  $f(R)$  cosmic acceleration that evade solar system tests*, *Phys. Rev. D* **76** (2007) 064004.

[69] S.M. Carroll, M. Hoffman and M. Trodden, *Can the dark energy equation-of-state parameter  $w$  be less than  $-1$ ?*, *Phys. Rev. D* **68** (2003) 023509.

[70] S. Capozziello, R. D'Agostino and O. Luongo, *Extended gravity cosmography*, *Int. J. Mod. Phys. D* **28** (2019) 1930016.

[71] R. Bhagat, F. Tello-Ortiz and B. Mishra, *Tracing cosmic evolution through weyl-type  $f(Q,T)$  gravity model: Theoretical analysis and observational validation*, *Phys. Dark Univ.* **48** (2025) 101913.